IEEE Access
Multidisciplinary ⋮ Rapid Review ⋮ Open Access Journal

Received February 23, 2020, accepted March 14, 2020, date of publication March 17, 2020, date of current version March 31, 2020.

*Digital Object Identifier 10.1109/ACCESS.2020.2981546*

# Design Optimization of Redundantly Actuated Cable-Driven Parallel Robots for Automated Warehouse System

**FEI ZHANG, WEIWEI SHANG, (Senior Member, IEEE), BIN ZHANG, AND SHUANG CONG**

Department of Automation, University of Science and Technology of China, Hefei 230000, China

Corresponding author: Weiwei Shang (wwshang@ustc.edu.cn)

This work was supported in part by the National Natural Science Foundation of China under Grant 51675501 and Grant 51275500, in part by the State Key Laboratory of Robotics and System under Grant SKLRS-2018-KF-07, and in part by the Youth Innovation Promotion Association CAS under Grant 2012321.

**ABSTRACT** This study focuses on the optimization of the geometry configurations and mobile platform parameters of redundantly actuated cable-driven parallel robots (RA-CDPRs) for automated warehouse system (AWS). Owing to their potential structural advantages, RA-CDPRs are proposed to replace conventional stackers in AWS, to achieve a high payload mass and low cable tension in frequent automated retrieval/storage operations. To meet these operational requirements, the maximal payload criterion satisfying the wrench-feasible condition is used to determine the optimal geometry configuration. Based on the optimal geometry configuration, the minimal cable tension is designed as the other criterion for optimizing the mobile platform parameters of RA-CDPRs. The optimization method is validated on a 6-DOF RA-CDPR, and the optimal results are simulated and implemented under static equilibrium conditions. Both the simulation and experimental results verify the optimal results can significantly enhance the payload mass and decrease the cable tension of AWS.

**INDEX TERMS** Cable-driven parallel robots, geometry configuration selection, optimization design, automated warehouse system.

## I. INTRODUCTION

In the conventional automated warehouse system (AWS), the automated storage and retrieval system (AS/RS) has a significant effect on the performance of the overall intralogistics system, including the energy consumption, space utilisation, and operational efficiency. The AS/RS is extremely mature and reliable, reflecting the efforts of decades of mechanical design and engineering optimization. However, owing to its inherent mechanical structure, the AS/RS cannot move in three translational directions at the same time; thus, it is difficult to complete certain movements, particularly storage turnover. To solve these problems, cable-driven parallel robots (CDPRs) have been proposed to replace the conventional AS/RS for massive and frequent storage turnover in AWS. CDPRs are characterised by high speeds, heavy payloads, and low energy consumption, enabling them to complete the storage turnover efficiently.

CDPRs use cables instead of rigid links and control the mobile platform pose in the workspace by changing the length and tension of the cables. Compared with rigid links, cables can extend to a more distant space, which provides CDPRs with the ability to operate in large areas [1], [2]. By driving the mobile platform through cables, all the drive units, including motors and gear reducers, can be located on the base structure to decrease the mass and inertia. At present, many CDPR prototypes have been designed to perform various tasks, such as manufacturing operations for large-scale material [3], high-speed photography in stadiums [4], giant radio telescopes [5], and handling operations for heavy payloads in huge workspaces [6], among others [7]–[9]. Hassan and Khajepour [10] proposed a symmetric

The associate editor coordinating the review of this manuscript and approving it for publication was Luigi Biagiotti.

CDPR of a large-workspace manipulator for automated warehouse system, and the mobile platform parameters are optimized to enhanced the manipulator stiffness. Ramadan *et al.* [11] studied the operating cycle of the storage turnover for a CDPR stacker and decreased the runtime by 60%. Bruckmann *et al.* [12] analysed the performance of a CDPR in an AWS by means of a simulation experiment, and the results validated that the energy consumption was reduced by 37% compared with the conventional AS/RS. Thereafter, the energy consumption was reduced by optimizing the electrical hardware [13]. There are many optimization methods to reduce the energy consumption. Reducing the cable tension is a common method to optimise the energy consumption. Wang *et al.* [14] minimized the energy consumption of the CDPR in an AWS by optimizing the tension distribution of the cables. But it is difficult to get accurate estimation of the payload weight in AWS [15], and the low cable tension will reduce the out-of-plane stiffness and cause the unexpected vibrations. Jamshidifar *et al.* [16] proposed a robust control method to reduce undesired vibrations of the plannar AWS when keeping the cable tension low. Further, Rushton *et al.* [17] designed a multiaxis reaction system for vibriation control of the plannar AWS, and proposed a robust control method to reduce undesired vibrations in the plane and also out-of-plane. However, existing works on AWS lack optimization of the geometry configurations and mobile platform parameters for CDPRs.

In CDPRs, the geometry configuration is defined as the cable arrangement between the mobile platform and base structure, and the mobile platform parameters are defined as the relative positions of the cable attachment points on the mobile platform. In general, for an $n$ degrees of freedom (DOF) CDPR with $m$ cables, if $m > n + 1$, the CDPR is redundantly actuated [6]. Redundantly actuated CDPRs (RA-CDPRs) for AWS consist of a base structure, drive units, cables, and a mobile platform with a retractable fork. With redundant actuation, RA-CDPRs can move in multiple motion directions simultaneously and bear higher payloads. Based on the geometry, kinematics, and dynamic characteristics, several criteria, such as the wrench-feasible workspace (WFW), stiffness, and dexterity have been introduced to analyse the performance of RA-CDPRs [18], [19]. Bryson *et al.* [20] designed an optimization objective considering the WFW to select the geometry configurations of a cable-driven robot leg with redundant actuation. Zhang *et al.* [21] analysed the stiffness conditions and used the stable workspace criterion to optimise the mobile platform size. Abdolshah *et al.* [22] studied the base structure configuration of a novel RA-CDPR, and optimized the stiffness and dexterity criteria simultaneously. However, the above studies focused on the parameter optimization of a pre-selected geometry configuration and ignored the optimization selection of geometry configurations. In several works, such as [23]–[25], the geometry configuration selection was discussed during the design process, in which an initial geometry configuration was selected and the optimization process was begun by exploring the entire design space. Pusey *et al.* [26] selected different geometry configurations to optimise the workspace and accuracy of the mobile platform for a 6-DOF RA-CDPR. Tadokoro *et al.* [27] optimized the geometry configurations of the mobile platform by considering the symmetry of the cable arrangements. Furthermore, Gouttefarde *et al.* [6] analysed the WFW, and optimized the geometry configurations and structural parameters of a suspended RA-CDPR. However, the above methods are incomprehensive for the design optimization of RA-CDPRs applied in AWS, in which the task requirements should also be considered.

Hao and Merlet [28] proposed a multi-criteria optimization method of parallel robot parameters based on the interval analysis, and took nearly 48 hours to optimize the parameters of one configuration. Lou *et al.* [29] analyzed and compared the application effect of several optimization algorithms for kinematically optimal design of parallel robot, and found that the optimization algorithm based on stochastic solution has better convergence effect in the complex multi-objective optimization problem. The multi-objective optimization problem is a common problem in the optimization design of parallel robots, and many optimization algorithms based on stochastic solution have been proposed to solve the complex multi-objective optimization problem [30]–[33]. In this study, the task requirements for the storage/retrieval operation in the AWS are analysed and two optimization criteria are proposed for the design optimization of RA-CDPRs. One optimization criterion is defined as the maximal payload, which is based on the wrench-feasible condition, while the other is known as the minimal cable tension. Then, a two-step optimization method is designed. First, all the geometry configurations satisfying the task requirements are provided and the optimal one is selected using the maximal payload criterion. Second, by considering the minimal cable tension, the mobile platform parameters are further optimized according to the optimal geometry configuration in the first step. Following the two-step optimization process, the optimal geometry configuration and corresponding mobile platform parameters of the RA-CDPRs in the AWS are obtained. The optimization method is validated on a 6-DOF RA-CDPR, and the optimal results are simulated and implemented under static conditions. Both the simulation and experimental results verify the optimal results can significantly enhance the payload mass and decrease the cable tension of AWS.

The remainder of this paper is organised as follows. The static model of RA-CDPRs are formulated in the ''Static modelling of RA-CDPRs'' section. In the ''Optimization criteria'' section, two performance criteria are established according to the maximal payload and minimal cable tension, respectively. A two-step optimization method is presented in the ''Optimization method'' section. In the ''Optimization method implementation'' section, the optimization method is validated on an RA-CDPR, and the optimal geometry configuration and corresponding mobile platform parameters are obtained. In the ''Experimental results'' section, the optimization results are further verified in the simulation and

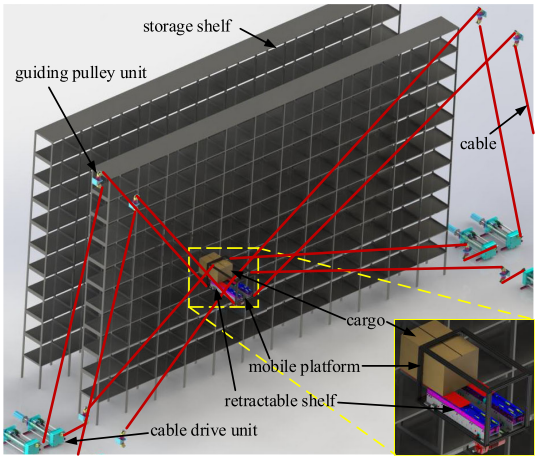


(a)

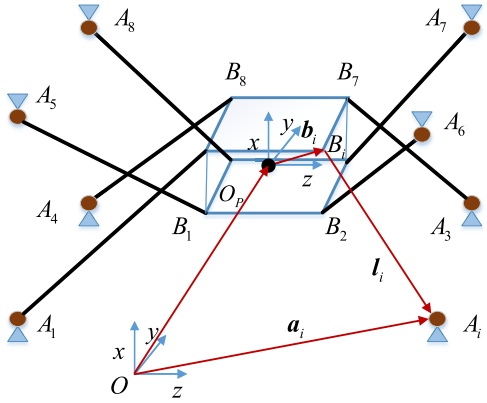


(b)

**FIGURE 1.** Illustrations of the RA-CDPR: (a) RA-CDPR used in AWS; (b) The kinematic coordinates of the RA-CDPR.

experiment under static conditions of AWS. Finally, several conclusions are presented.

## II. STATIC MODELLING OF RA-CDPRs

A 6-DOF RA-CDPR used in AWS is actuated by 8 cables, and each cable comes out from a drive unit through a guiding pulley unit to the anchor point on the mobile platform. A retractable fork used to store/retrieve cargo is equipped on the mobile platform, as shown in Figure 1a. For the convenience of description, the kinematic coordinates of the RA-CDPR are given in Figure 1b. Since the cable mass is much smaller than that of the mobile platform and payload, the cable is assumed to be a light rigid link. The global coordinate frame is denoted as $\{O\}$, and the local coordinate frame is denoted as $\{O_P\}$ which is attached to the geometry center of the mobile platform. Moreover, the pose of the mobile platform is described by $\boldsymbol{p} = [x, y, z, \alpha, \beta, \phi]^T$.

Vector $\boldsymbol{a}_i$ denotes attachment point $A_i$ on the base structure in the global frame, vector $\boldsymbol{b}_i$ denotes the attachment point $B_i$ on the mobile platform in the frame $\{O_P\}$ and vector $\boldsymbol{l}_i$ denotes the vector of the $i$th cable in the global frame. Thus, the static equilibrium equation of the RA-CDPRs can be described as

$$\boldsymbol{A} \cdot \boldsymbol{T} + \boldsymbol{w} = \boldsymbol{0}, \tag{1}$$

where vector $\boldsymbol{T} = [T_1, T_2, \ldots, T_8]^T$ represents the tension of cables. Vector $\boldsymbol{w} = [\boldsymbol{f}, \boldsymbol{t}]^T$ represents the external wrench, vector $\boldsymbol{f}$ denotes the external force and vector $\boldsymbol{t}$ denotes the external moment that applied on the mobile platform. $\boldsymbol{A}$ is the transpose of the Jacobian matrix expressed as

$$\boldsymbol{A} = \begin{bmatrix} \boldsymbol{u}_1 & \boldsymbol{u}_2 & \ldots & \boldsymbol{u}_8 \\ \boldsymbol{b}_1 \times \boldsymbol{u}_1 & \boldsymbol{b}_2 \times \boldsymbol{u}_2 & \ldots & \boldsymbol{b}_8 \times \boldsymbol{u}_8 \end{bmatrix}, \tag{2}$$

where vector $\boldsymbol{u}_i = \frac{\boldsymbol{l}_i}{\|\boldsymbol{l}_i\|} = \frac{\boldsymbol{a}_i - \boldsymbol{p} - \boldsymbol{R}\cdot\boldsymbol{b}_i^P}{\|\boldsymbol{a}_i - \boldsymbol{p} - \boldsymbol{R}\cdot\boldsymbol{b}_i^P\|}$, $i = 1, 2, \ldots, 8$. Here, $\boldsymbol{b}_i^P$ denotes the position of point $B_i$ in the frame $\{O_P\}$. Matrix $\boldsymbol{R}$ is the rotation matrix from the frame $\{O_P\}$ to the frame $\{O\}$. Cable tension are subjected to the minimal and the maximal admissible values. The maximal value ($T_{max}$) is necessary to consider the mechanical limits. The minimal value ($T_{min}$) must be nonnegative because the cables cannot be compressed. The general solution for Eq. (1) can be written as

$$\boldsymbol{T} = -\boldsymbol{A}^*\boldsymbol{w} + \boldsymbol{H}\boldsymbol{\lambda}_H, \tag{3}$$

where $\boldsymbol{A}^*$ is the Moore-Penrose Pseudo-Inverse of matrix $\boldsymbol{A}$, $\boldsymbol{A}^*\boldsymbol{w}$ is the minimal norm solution of Eq. (1), and $\boldsymbol{H}$ is the null-space or kernel of $\boldsymbol{A}$ such that $\boldsymbol{AH} = \boldsymbol{0}$. To find all feasible solutions is a non-trivial problem, as the null-space spans a 2-dimensional hyperspace ($\boldsymbol{\lambda}_H$) and different solutions are existent. The tension distribution can be derived by quadratic optimization algorithms [34], and can be written as follows:

$$\begin{aligned} &\min_{\boldsymbol{T}} \left(\frac{1}{2}\boldsymbol{T}^T\boldsymbol{Q}\boldsymbol{T} + \boldsymbol{f}_{ref}^T\boldsymbol{T}\right) \\ &\text{subject to: } \boldsymbol{T}_{min} \le \boldsymbol{T} \le \boldsymbol{T}_{max}, \\ &\qquad \boldsymbol{A}\cdot\boldsymbol{T} + \boldsymbol{w} = \boldsymbol{0}, \end{aligned} \tag{4}$$

where $\boldsymbol{Q}$ is chosen as a identity matrix. $\boldsymbol{f}_{ref}^T$ is a reference force used to adjust the tension level of the cable tension $\boldsymbol{T}$. The objective function Eq. (4) is subject to the following constraints: $\boldsymbol{T}_{min} \le \boldsymbol{T} \le \boldsymbol{T}_{max}$ and $\boldsymbol{A}\cdot\boldsymbol{T} + \boldsymbol{w} = \boldsymbol{0}$. A third-party optimization toolbox, the OPTI toolbox [35] is used to solve Eq. (4). The solution speed of the OPTI toolbox is 3 to 10 times faster than the optimization toolbox in MATLAB, and the solution time is about 2.5ms on a desktop computer with I7-4470-3.4Ghz.

## III. OPTIMIZATION CRITERIA

In the application of AWS, several essential performance criteria exist for RA-CDPRs, such as the energy consumption, maximal payload, and WFW. Our goal is to evaluate the overall performance of the storage/retrieval operations, and then improve the overall performance by optimizing the geometry configurations and mobile platform parameters. To this end, we introduce two optimization criteria, which are defined as the maximal payload and minimal cable tension considering the wrench-feasible condition.

### A. WORKING STATE ANALYSIS

Under ideal conditions, the mobile platform centre of gravity (CoG) and geometric centre should be at the same point. However, owing to the influence of the payload, the weight

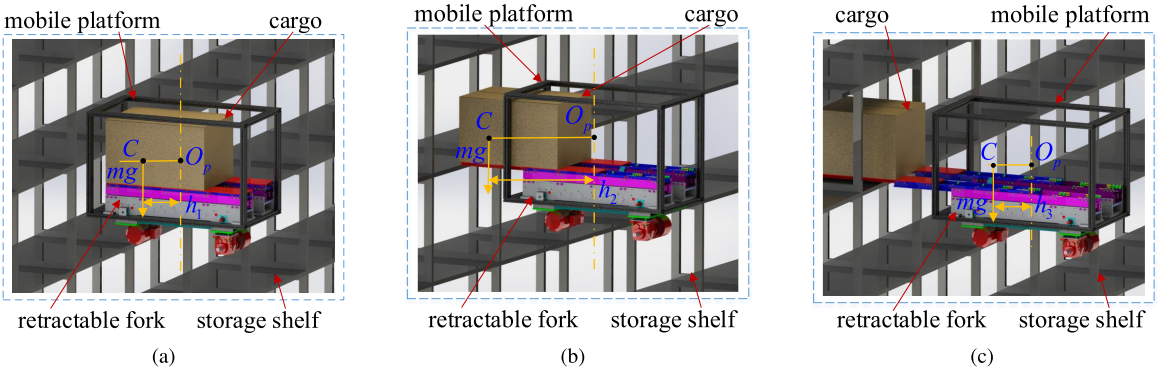


**FIGURE 2.** Illustrations of working status of retractable fork: (a) the retractable fork is at rest; (b) the retractable fork moves between the mobile platform and storage shelf; and (c) the retractable fork has reached the storage shelf.

distribution of the mobile platform is not uniform, so the CoG position of the mobile platform changes. In this study, the points $O_p$ and $C$ represent the mobile platform geometric centre and the CoG, respectively, as illustrated in Figure 2, where $h_1$, $h_2$, and $h_3$ denote the respective distances between points $O_p$ and $C$. The mobile platform can perform the operation of storage/retrieval of cargos on the storage shelf through the retractable shelf. The working state of the retractable fork can be divided into three parts, which are described as follows.

When the retractable fork is at rest state, as illustrated in Figure 2a, the mobile platform can move freely in the workspace. The distance $h_1$ between points $C$ and $O_p$ is actually small, because the payload is within the mobile platform, so it has little effect on the positional change of the CoG of the mobile platform. It is assumed that this maximum distance ($h_1$) should be equal to 1/2 of the mobile platform depth under extreme conditions.

The working state, in which the retractable fork moves between the mobile platform and the storage shelf, and the mobile platform is at rest, is illustrated in Figure 2b. Under this condition, the CoG of the mobile platform and the payload may be outside the mobile platform structure; thus, the moment applied to the mobile platform is much greater than that at the rest status. The magnitude of this moment is only related to the mass of the payload and distance ($h_2$) between points $C$ and $O_p$. Under extreme conditions, the distance ($h_2$) between the mobile platform geometric center and the CoG is at a certain distance $h_2 = r$. Here, $r$ denotes the distance between the mobile platform geometric center and the storage shelf.

Figure 2c illustrates the case where one end of the retractable fork is on the storage shelf, at which point the storage shelf has been subjected to the force of the retractable fork and payload. In contrast, the force exerted by the payload on the mobile platform is significantly reduced. At this time, the offset ($h_2$) owing to the change in the CoG position of the payload has been reduced and is less than the distance ($r$).

Hence, when changing the retractable shelf position, the CoG position of the mobile platform will change accordingly. Moreover, owing to the weight of the cargo, the CoG position of the mobile platform will change drastically. In this paper, the required wrench set (RW) denotes the wrench set that the cables must apply to the mobile platform to balance the force and moment generated by the weight of the payload and mobile platform. Determining the variation range of the RW is related to the normal operation of the CDPR and the safety of the entire system. By analysing the working state of the retractable fork, it is easy to establish the boundary range of the RW, which will be described in detail in the ''maximal payload'' section.

### B. MAXIMAL PAYLOAD

The WFW of RA-CDPRs consists of a set of poses at which cables can generate all-positive tensions at the mobile platform for a given external wrench ($\boldsymbol{w}$), and $\boldsymbol{w}$ can be defined by the available wrench (AW)

$$\mathrm{AW} = \{\boldsymbol{w} = -\boldsymbol{A}\boldsymbol{T} | \boldsymbol{T}_{min} \leq \boldsymbol{T} \leq \boldsymbol{T}_{max}\}, \tag{5}$$

where all components of the 8-dimensional vector $\boldsymbol{T}_{min}$ are equal to the minimal admissible cable tension $T_{min} > 0$, and all components of $\boldsymbol{T}_{max}$ are equal to $T_{max}$. The definition of the RW set is directly related to the actual application task, and the mobile platform pose is wrench-feasible when RW $\subseteq$ AW, meaning that the cables can generate any wrenches in RW and the cable tensions meet the constraints $\boldsymbol{T}_{min} \leq \boldsymbol{T} \leq \boldsymbol{T}_{max}$. For a given operation task, the RW is related to the payload weight and the position of retractable fork. As illustrated in Figure 3, the mobile platform can perform the cargo storage/retrieval operation by means of the retractable fork. When changing the position of retractable fork, the CoG of the mobile platform and payload will change accordingly. The point $P$ denotes the geometric centre of the mobile platform, while $C$ denotes the CoG. The overall mass of the mobile platform and the cargo is denoted by $m$, and $O_p$ indicates the coordinate frame origin.

The vector $\boldsymbol{w} = [f_x\ f_y\ f_z\ t_x\ t_y\ t_z]^T$ describes the external wrench that the cables must apply to balance the overall weight, and it satisfies

$$f_x = f_y = t_z = 0,\ f_z = mg,\ \sqrt{t_x^2 + t_y^2} = mgh, \tag{6}$$

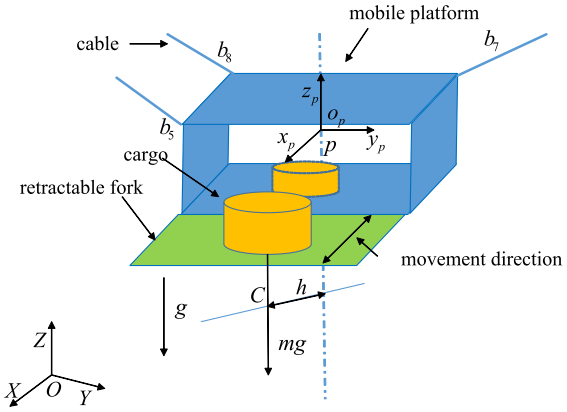


**FIGURE 3.** Cargo storage/retrieval by mobile platform.

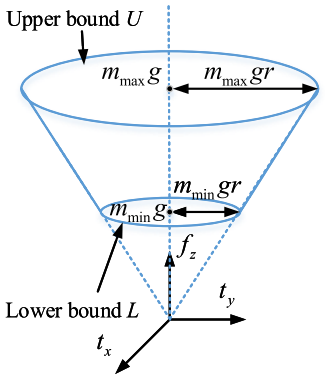


**FIGURE 4.** RW of a convex hull.

where $f_x, f_y$, and $f_z$ are forces along the axes of the frame $O_p$, while $t_x$, $t_y$, and $t_z$ are the moments about the $X_p$, $Y_p$, and $Z_p$ axes, respectively. Furthermore, $h$ denotes the horizontal distance between points $P$ and $C$ of the mobile platform, that is dependent on the cargo position and mass. The position of $C$ and payload mass ($m$) are not precisely known but are subject $0 \leq h \leq r$ and $m_{min} \leq m \leq m_{max}$. Here, $r$ denotes the maximum distance between points $C$ and $P$. Moreover, $m_{min}$ is the minimal mass of the empty mobile platform and $m_{max}$ is the maximal mass of the mobile platform with the heaviest cargo. RW has been discussed in detail in [36], and is described here according to the definition in the paper. Thus, the RW can be defined as the set of wrenches

$$\mathrm{RW} = \{\boldsymbol{w} | f_x = f_y = 0, m_{min}g \leq f_z \leq m_{max}g, \quad t_z = 0, \quad 0 \leq \sqrt{t_x^2 + t_y^2} \leq mgr\}. \tag{7}$$

It is not difficult to conclude that RW is a convex hull, as shown in Figure 4. The lower bound ($L$) and the upper bound ($U$) of RW can be expressed by

$$L = \{\boldsymbol{w} | f_x = f_y = t_z = 0, f_z = m_{min}g, \quad 0 \leq \sqrt{t_x^2 + t_y^2} \leq m_{min}gr\}, \tag{8}$$

$$U = \{\boldsymbol{w} | f_x = f_y = t_z = 0, f_z = m_{max}g, \quad 0 \leq \sqrt{t_x^2 + t_y^2} \leq m_{max}gr\}. \tag{9}$$

Therefore, RW $\subseteq$ AW is equivalent to both the upper bound ($U$) and lower bound ($L$) being entirely contained within AW. In our optimization process, the purpose is to improve the maximal payload of the RA-CDPR. The value of $h$ cannot be obtained precisely, because the exact position of the CoG is unknown. However, $r$ is related to the actual task and less than the longest distance of the retractable fork movement, namely $0 \leq r \leq D_s/2$, where $D_s$ denotes the distance between two shelves. Each piece of cargo needs to be transported between the platform and shelves using a retractable fork. Moreover, $r$ can be set as $r = D_s/2$ to guarantee safety to a certain extent. Thus, the maximal payload ($m_{max}$) can easily be determined, and RW can be rewritten as

$$f_x = f_y = 0, \ f_z = m_{max}g, \ t_x = m_{max}gr\cos(\theta), \quad t_y = m_{max}gr\sin(\theta), \ t_z = 0, (-\pi/2 \leq \theta \leq \pi/2), \tag{10}$$

where $\theta$ is the angle between the $X-$axis and the line from point $C$ to the geometric centre point $P$. Thus, $U \subseteq$ AW if and only if all the components in Eq. (10) satisfy the linear inequality proposed in [36]:

$$\boldsymbol{n}^T \boldsymbol{w}_v \leq \boldsymbol{d}, \quad v = 1, 2, 3, \ldots, 2^6. \tag{11}$$

Here, $\boldsymbol{n}$ is a matrix in which the $i$th column is $\boldsymbol{n}_i = [n_{if_x} \ n_{if_y} \ n_{if_z} \ n_{it_x} \ n_{it_y} \ n_{it_z}]^T$, representing a unit normal vector of a hyper-plane and pointing towards the exterior of the zonotope. The $i$th component ($d_i$) of $\boldsymbol{d}$ is the dot-product of the normal vector $\boldsymbol{n}_i^T$ and a known point $\boldsymbol{h}_i$ included in the hyper-plane. Thus, the normal vector $\boldsymbol{n}$ and point $\boldsymbol{h}_i$ can be expressed as

$$\boldsymbol{n}_i = (\boldsymbol{a}_1 \times \boldsymbol{a}_2 \times \cdots \times \boldsymbol{a}_5)/(\|\boldsymbol{a}_1 \times \boldsymbol{a}_2 \times \cdots \times \boldsymbol{a}_5\|), \tag{12}$$

$$\boldsymbol{h}_i = H_d \boldsymbol{n}_i + \boldsymbol{A}\boldsymbol{T}_{min}, \tag{13}$$

where $\{\boldsymbol{a}_1, \ldots, \boldsymbol{a}_5\}$ is a set of 5 linear independent column vectors of matrix $\boldsymbol{A}$, and the shift distance can be expressed as

$$H_d = max(\textstyle\sum_{j=1}^{3} I_j(\bar{T}_j - \underline{T}_j)\boldsymbol{a}_j^T \boldsymbol{n}_j, I_j = [0, 1]). \tag{14}$$

With the notations in Eq. (5) and Eq. (10), all components in RW satisfy the inequality in Eq. (11) if and only if

$$(n_{vf_z} + n_{vt_x} r\cos(\theta) + n_{vt_y} r\sin(\theta))m_{max}g \leq d_v, \tag{15}$$

which can be further expressed as

$$m_{max} \leq \frac{d_v}{(n_{vf_z} + r(n_{vt_x}\cos(\theta) + n_{vt_y}\sin(\theta)))g}. \tag{16}$$

The right side of Eq. (16) is a function of $\theta$, which has the minimal value when

$$\sin(\theta) = n_{vt_y}/\sqrt{n_{vt_x}^2 + n_{vt_y}^2}, \tag{17}$$

$$\cos(\theta) = n_{vt_x}/\sqrt{n_{vt_x}^2 + n_{vt_y}^2}. \tag{18}$$

Thus, Eq. (16) is true if

$$m_{max} \leq \frac{d_v}{(n_{vf_z} + r\sqrt{n_{vt_x}^2 + n_{vt_y}^2})g}. \tag{19}$$

Hence, to ensure that the maximal payload ($m_{max}$) satisfies all of the inequalities in Eq. (19), $m_{max}$ can further be determined as

$$m_{max} = \min_{v} \frac{d_v}{(n_{vf_z} + r\sqrt{n_{vt_x}^2 + n_{vt_y}^2})g}. \tag{20}$$

In fact, it is not necessary to prove that $L \subseteq$ AW. Hence, the optimization goal of the maximal payload considered here can be written as

$$\begin{aligned} \max m_{max} &= \min_{v} \frac{d_v}{(n_{vf_z} + rg\sqrt{n_{vt_x}^2 + n_{vt_y}^2})g}, \\ & v = 1, \ldots, N_i \cdot N_p. \\ \text{subject to } & K_c \neq 1 \text{ and } \boldsymbol{b_i} \in [\boldsymbol{b}_{min}, \boldsymbol{b}_{max}] \end{aligned} \tag{21}$$

where $N_i = 2^6$ is the number of inequalities in $\boldsymbol{Nw} \leq \boldsymbol{d}$ and $N_p$ is the number of poses in the discretised workspace. The position vector $\boldsymbol{b}_i = [b_ix, b_iy, b_iz]$ denotes the cable attachment point on the mobile platform. Furthermore, the variation range of the mobile platform parameters is expressed as $[\boldsymbol{b}_{min}, \boldsymbol{b}_{max}]$. The collision-detection algorithm used here was obtained from [37], and $K_c$ denotes cable-cable, cable-platform, and cable-obstacle collisions. When a collision occurs, $K_c = 1$.

### C. MINIMAL CABLE TENSION

In this section, we aim to achieve lower energy consumption by optimizing the cable tension. In general, the cable tension of the RA-CDPRs depends on the mobile platform and cargo weight, as well as the mobile platform pose and geometry configuration. As the mass of the cargo increases, the average cable tension will inevitably increase for a given pose and geometry configuration. The WFW of the RA-CDPR will also be affected or even reduced by the cargo mass. In such situations, the optimization criterion must be defined to synthesise all aspects of the desired criterion and prioritise the set of criterion parameters according to their relative importance to the outcome.

For RA-CDPRs used in AWS, the overall optimization criterion is to optimise the mobile platform parameters and geometry configuration, which can complete the turnover of heavy cargo with minimal cable tension. To accomplish this, the optimization criterion should consider that the desired workspace of the actual task requirements must be included in the WFW, and the cable tension should be minimised.

To consider these design goals synthetically, the optimization criterion uses the natural log of a nonlinear combination of the workspace criterion $P_w$ and average cable tension $\tau$ [20]. The optimization criterion for the cable tension is designed as follows:

$$\begin{aligned} &\text{minimize } P_\tau = \ln(\tau_{avg}(\varepsilon + P_w)/\mu), \\ &\text{subject to } K_{collision} \neq 1, \end{aligned} \tag{22}$$

where $P_\tau$ denotes the cable tension criterion and $\tau_{avg}$ denotes the average cable tension of $N_p$ poses in the desired workspace, which can be calculated as

$$\tau_{avg} = mean(\tau_1, \tau_2, \ldots, \tau_j, \ldots, \tau_{N_p}), \tag{23}$$

where $\tau_j = mean(\boldsymbol{T}^j)$ can be determined by Eq. (4) and $\boldsymbol{T}^j = [T_1^j, T_2^j, \ldots, T_8^j]^T, j = 1, \ldots, N_p$. In Eq. (22), $P_w$ denotes the percentage of the desired workspace in which the cable tension cannot meet the wrench-feasible condition, which can be expressed as

$$P_w = 1 - \frac{WFW \bigcap W_d}{W_d}, \tag{24}$$

where $W_d$ is the desired workspace of the task requirements. When the intersection of WFW and $W_d$ is empty, $P_w = 1$. When $W_d$ is entirely included in the WFW, $P_w = 0$ and the cable tension criterion is maintained.

To reduce the execution time of the optimization algorithm, the number ($N_p$)of poses is generally small. Since the criterion $P_w$ is usually small in value, the curve slope of the tension criterion ($P_\tau$) will be larger when the cable tension value ($\tau_{avg}$) is smaller. Thus, the smaller cable tension will also have a greater impact on the tension criterion ($P_\tau$) with the same $P_w$. Figure 5 illustrates the values of criterion $P_\tau$ versus the average cable tension for several values of $P_w$. When the three curves in the Figure 5 are under the same average cable tension ($\tau_{avg}$), the influence of the workspace criterion on the tension criterion ($P_\tau$) will be further amplified. Therefore, using the optimization objective equation of the natural log function can improve the resolution and sensitivity of the optimization cirterion ($P_\tau$) to the cable tension, which just meets the optimization objective of RA-CDPRs with smaller cable tension. If the optimization criterion is designed as a linear combination of the $P_w$ and $\tau_{avg}$, it will be very difficult to select the weighting coefficients in the optimization criterion to adjust the relative influence of the two performance criteria. Under this definition, the WFW becomes the primary condition for optimization. Moreover, $\varepsilon$ and $\mu$ are constant to maintain the criterion $P_\tau$ within the desired range. The parameter $\varepsilon$ can be set to $0 < \varepsilon \leq 0.1$, and the parameter $\mu$ can be set to $\mu = 0.2\tau_{avg}$, so that the final output result is $0 < P_\tau$.

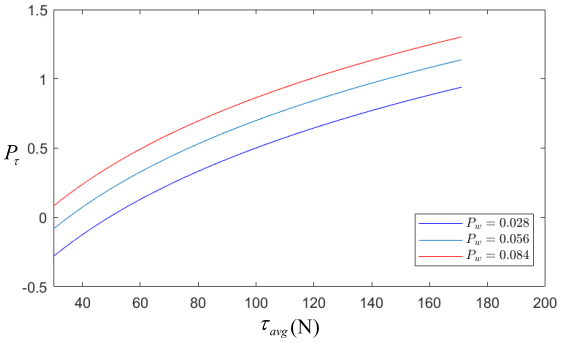


**FIGURE 5.** Value of criterion $P_\tau$ versus average cable tension $\tau_{avg}$ for several workspace performance values ($P_w$).

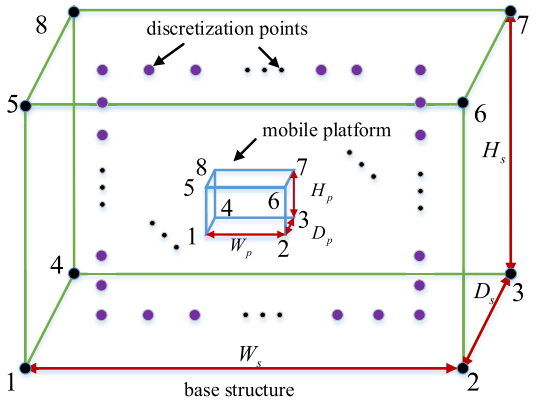


**FIGURE 6.** Illustration of structure.

## IV. OPTIMIZATION METHOD

### A. OPTIMIZATION OF GEOMETRY CONFIGURATIONS

In the first phase of the optimization method, all possible geometry configurations are generated for optimization. These geometry configurations are arranged according to the maximal payload criterion, and their optimal mobile platform parameters will be selected as the initial parameters for the second phase of the optimization method. To this end, three steps of the first phase of the optimization method are designed, as follows.

Define geometry configurations: A 6-DOF RA-CDPR actuated by eight cables is considered in this case. The mobile platform and base structure are both usually modelled as cuboids, and each cable extends from a vertex of the base cuboid to a vertex of the mobile platform. As indicated in Figure 6, $W_s$, $H_s$, and $D_s$ denote the width, height, and depth of the base structure, respectively. Similarly, $W_p$, $H_p$, and $D_p$ denote the width, height, and depth of the mobile platform. The storage shelves are modularly designed and assembled to maximize the space utilization of the AWS. In order to optimize the space utilization of the AWS, the width ($W_s$) and height ($H_s$) of the base structure of RA-CDPR are maximized, and the distance ($D_s$) between the two shelves is minimized. Further, considering the safe distance of collision, a safe distance will be reserved for the depth of the mobile platform, which can be taken as $D_p = D_s - d_c$, here $d_c$ denotes the safe collision distance. In addition, the depth ($D_f$) of the storage shelf is also a standard parameter of modularization, which can be taken as 0.6m, 0.8m and so on. The working distance of the retractable fork must be longer than the depth ($D_f$) of the shelf. Hence, the depth ($D_p$) of the mobile platform must satisfy $D_f \leq D_p \leq D_s - d_c$. When $D_f = D_p = D_s - d_c$, the distance ($D_s$) between the two shelves is the minimal, and the space utilization is the maximal. Based on these above factors, some parameter dimensions of the RA-CDPR can be determined including $W_s$, $H_s$, $D_s$ and $D_p$. It is generally known that the geometry configurations of the base structure and mobile platform exhibit certain symmetry properties. In this study, only the parameters $\{W_p, H_p\}$ of points {5, 6, 7, 8} of the mobile platform are optimized.

**TABLE 1.** The cable connection rules between the mobile platform and the base structure.

| Cable connection in configuration matrix | | | |
|---|---|---|---|
| $\boldsymbol{G}_{i,1} \neq 7$ | $\boldsymbol{G}_{i,2} \neq 8$ | $\boldsymbol{G}_{i,3} \neq 5$ | $\boldsymbol{G}_{i,4} \neq 6$ |
| $\boldsymbol{G}_{i,5} \neq 3$ | $\boldsymbol{G}_{i,6} \neq 4$ | $\boldsymbol{G}_{i,7} \neq 1$ | $\boldsymbol{G}_{i,8} \neq 2$ |

Generate geometry configurations: Prior to connecting the base structure and mobile platform with cables, several connection rules should be defined. The matrix $\boldsymbol{G}$ with a dimension of $8! \times 8$ is used to describe all possible cable arrangements, and the $i$th row $\boldsymbol{G}_i$ of $\boldsymbol{G}$ contains the $i$th type of the possible geometry configurations. When the element $\boldsymbol{G}_{i,j} = k, k = \{1, \ldots, 8\}$, this indicates that the cable is drawn from the $j$th vertex of the base structure to the $k$th vertex of the mobile platform. To generate valid cable arrangements, the following rules should be considered: 1) all vertexes of the base structure must be connected, which means that $\boldsymbol{G}_i \neq \varnothing$; and 2) all vertexes of the mobile platform must be connected, which means that $\boldsymbol{G}_{i,j} = k, k = \{1, \ldots, 8\}$.

Under the above rules, all possible cable arrangements can be generated. The dimension of $\boldsymbol{G}$ is $8! \times 8$ and the number of geometry configurations is $8! = 40320$. Moreover, it is necessary to consider the symmetry when designing the cable arrangements. In this cuboid structure, the $j$th vertex of the base structure has a symmetrical vertex, and the latter is numbered as $8 - j + 1$. Therefore, to reflect the symmetry of the cable arrangements, we only retain the types of $\boldsymbol{G}$ such that $\boldsymbol{G}_{i,j} + \boldsymbol{G}_{i,m-j+1} = 9$. That is, the final number of geometry configurations is 384.

Furthermore, the task requirements of the mobile platform should be analysed to determine the connection rules further. In the storage/retrieval operation, there is no crossing or interference between the cable and the $X-Y$ plane, because the retractable fork exhibits movement on the $X-Y$ plane. Therefore, certain cable arrangements will be abandoned based on the following connection rules in Table 1. All the connection rules can easily be obtained by analysing the task requirement, as shown in Figure 7. In the end, the number of effective cable arrangements is 132. Owing to the two aspects above, the number of geometry configurations is significantly reduced, which can also decrease the time consumption of the optimization process.

Solve the optimization problem: In this step, each geometry configuration and its mobile platform parameters are optimized by a stochastic optimization algorithm. The maximal payload ($m_{max}$) is a function of the mobile platform parameters, but it is difficult to obtain a Jacobian function for the design variables in the vector $\Delta\boldsymbol{p}$. To solve this problem, the Tabu search algorithm is used, as shown in Figure 8. $\{TL\}$ denotes the tabu list, and the length of the tabu list is $L$. Vector $\Delta\boldsymbol{p}_k$ denote the $k$th randomly selected parameters of the mobile platform, and $K$ is the maximal iterations of the optimization algorithm. Moreover, $\Delta\boldsymbol{p}.d_n$ represents the $n$th domain solution of vector $\Delta\boldsymbol{p}_k$, and the maximal number of domain solutions is $N$, and $\{\Delta\boldsymbol{p}_b\}$ denotes the optimal

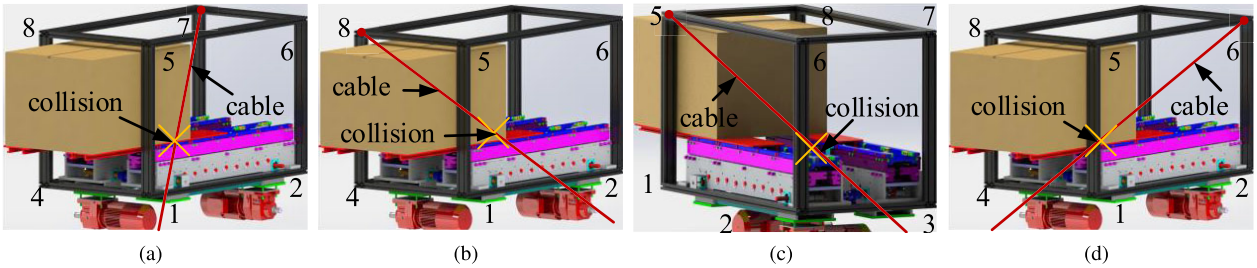


**FIGURE 7.** Interference collision occurs between the mobile platform and the cable in several cable connection arranegements: (a) $G_{i,1} = 7$; (b) $G_{i,2} = 8$; (c) $G_{i,3} = 5$; and (d) $G_{i,4} = 6$.

solution set. $\boldsymbol{G}_i^1$ represents the $i$th geometry configuration, and the maximal value of $i$ is 132 in the first phase optimization. The Tabu search algorithm was introduced by Glover in [38], and uses intelligent guidance to avoid falling into the local optimal solutions in the solution space. It has a memory containing the already determined solutions to prevent the optimization process from performing an invalid loop. The stop iteration condition used here can be set to the maximal number of loops and cannot be improved following the multi-step optimization.

All the effective geometry configurations of the RA-CDPR are generated in step 2, and optimized by the Tabu search algorithm at each pose of the desired workspace ($W_d$). At the end of the first phase of the optimization method, all geometry configurations will be ranked in descending order, according to the maximal payload criterion. Several geometry configurations can be discarded based on this arrangement, and the mobile platform parameters of the remaining configurations will be optimized further in the second phase of optimization. The optimal parameters here will be used as the initial parameters of the geometry configurations for the second phase of optimization.

### B. OPTIMIZATION OF MOBILE PLATFORM PARAMETERS

In the first phase of the optimization method, the feasible geometry configurations are obtained by considering the maximal payload ($m_{max}$), following which the mobile platform parameters are further optimized with the selected geometry configuration in the second phase. The optimization objective used here is illustrated in Eq. (22), and the steps of the second phase can be briefly described in Figure 9.

Initialise the optimization algorithm: Let matrix $\boldsymbol{G}^1$ denote all of the geometry configurations that are optimized in the first phase of the optimization method. The matrix $\boldsymbol{G}^2$ denotes all of the geometry configurations that are optimized in the second phase of the optimization method, and $\boldsymbol{G}^2$ is an empty set in the beginning. The vector $\boldsymbol{P}^1$ denotes the optimal parameters generated in the first phase, while the vector $\boldsymbol{P}^2$ describes the parameters optimized in the second phase, which is also an empty set in the beginning.

Optimise the mobile platform parameters: Obtain a vector $\boldsymbol{G}_i^1$ from the matrix $\boldsymbol{G}^1$, and the corresponding $\boldsymbol{P}_i^1$ will be obtained as the initial parameters of the Tabu search algorithm ($Ts(\boldsymbol{G}_i^1, \boldsymbol{P}_i^1)$). When the loops reach the maximal number or the multiple-loop calculations cannot achieve further

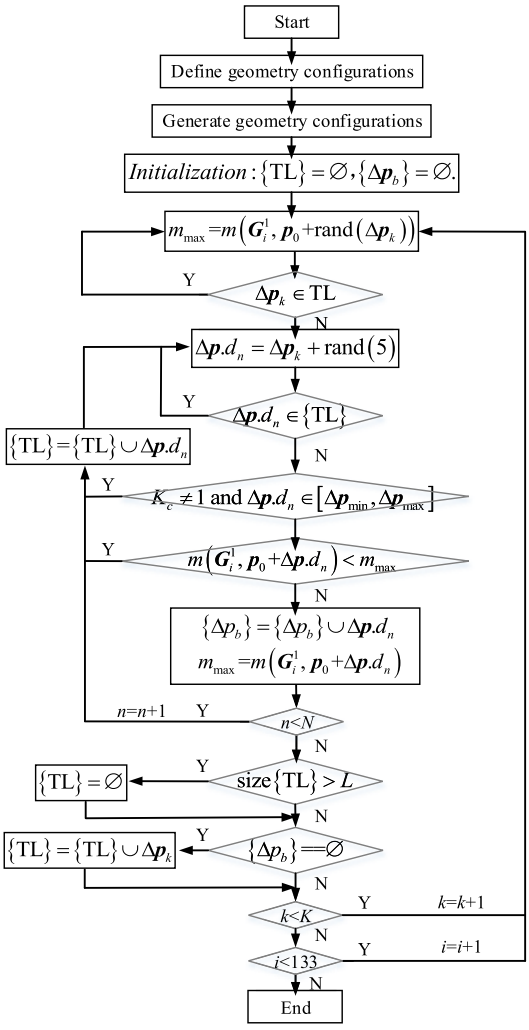


**FIGURE 8.** Flow chart of the first phase optimization.

improvement, the Tabu search algorithm will stop and the current optimization parameters will be exported.

Save the optimization results: The optimal parameters obtained from the Tabu search algorithm will be stored in $\boldsymbol{P}_i^2$. Finally, the entire process will exit when $\boldsymbol{G}^1 = \varnothing$; otherwise, it will re-extract a vector $\boldsymbol{G}_{i+1}^1$ from the matrix $\boldsymbol{G}^1$ and proceed to the next iteration.

Following the optimization process, the values of $m_{max}$ and $P_\tau$ can be obtained for the corresponding geometry configuration and mobile platform parameters. Prior to designing the

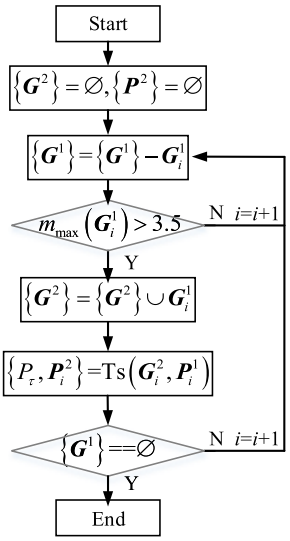


**FIGURE 9.** Flow chart of the second phase optimization.

RA-CDPR, the optimal geometry configuration is selected based on the maximal payload ($m_{max}$). However, there may be multiple configurations that meet the requirements, and among these, the most optimal is further selected according to the minimal cable tension criterion ($P_\tau$).

## V. OPTIMIZATION METHOD IMPLEMENTATION

In this section, the overall optimization method presented in "Optimization method" section is validated on a 6-DOF RA-CDPR, and the optimal geometry configuration and mobile platform parameters are obtained.

### A. INPUT DATA

The 6-DOF RA-CDPR is driven by eight cables. Several input data and the basic constraints are described as follows.

#### 1) WORKSPACE DIMENSION

The dimension of the base structure is dependent on the actual dimension of the shelves, which is 1500mm × 1800mm × 500mm ($W_s \times H_s \times D_s$). The desired workspace is defined by scaling of this cuboid: 80% of the width and 80% of the height. There are $9 \times 9 = 81$ discretization points are uniformly distributed on the square plane of the area 1200mm × 1440mm, which coincides with the vertical plane of the geometric center of the RA-CDPR, as shown in Figure 6.

#### 2) MOBILE PLATFORM DIMENSION

The dimension of the mobile platform is set to 200mm × 150mm × 300mm ($W_p \times H_p \times D_p$). To validate the optimal parameters, the minimal variation of the mobile platform parameters $\triangle \boldsymbol{p} = [\triangle W_p, \triangle H_p]$ is set to 1mm, while the range of $\triangle p_i$ is set to $\triangle p_i \in [-50, 50]$mm.

#### 3) PAYLOAD MASS AND CABLE TENSION

The mobile platform mass $m_{min} = 0.5$kg, and the authorised maximal payload mass $m_{max} = 3.5$kg. The cables are Dyneema cable with a diameter of 1.5mm, and the maximal tension is 750**N**. Dyneema cable is characterized by lightweight, extremely high strength, very low stretch, abrasion resistant and flexible, which can be applied in applications with heavy payload, high process velocities and high accelerations [39]. Considering the maximal tension of the cable and maximal payload of the mechanical components, the maximal admissible cable tension $T_{max} = 500$N. Moreover, to prevent sagging of the cables, the minimal cable tension $T_{min} = 5$N.

**TABLE 2.** Geometry configurations and parameters obtained in first phase of optimization method.

| | Geometry configuration types | | | | |
|---|---|---|---|---|---|
| | No. 30 | No. 25 | No. 6 | No. 1 | No. 81 |
| $m_{max}$ (kg) | 5.909 | 5.291 | 4.704 | 4.701 | 2.003 |
| $\triangle \boldsymbol{p}$ (mm) | [-50 30] | [29 -41] | [25 20] | [7 -34] | [-15 13] |

**TABLE 3.** Optimization results obtained in second phase of optimization method.

| | Geometry configuration types | | | |
|---|---|---|---|---|
| | No. 30 | No. 25 | No. 6 | No. 1 |
| $P_\tau$ | 0.0747 | 0.1003 | 0.0757 | 0.1938 |
| $\triangle \boldsymbol{p}$ (mm) | [-21 25] | [36 -23] | [9 -7] | [36 -2] |

#### 4) PARAMETERS OF THE OPTIMIZATION ALGORITHM

The maximal loops of the Tabu search algorithm is 500, and the sizes of the Tabu list and candidate list are set to 10 and 20, respectively. The computation time of the optimization algorithm is affected by these parameters; thus, the algorithm parameters need to be adjusted according to the solution space. The cable tension criterion factor $\varepsilon$ is set to 0.1, while $\mu$ is set to 10.

### B. OPTIMIZATION RESULTS

Following the first phase of the optimization method, the geometry configurations are arranged in descending order by the maximal payload ($m_{max}$), five of which are presented in Table 2. Only four geometry configurations with a maximal payload ($m_{max}$) greater than 3.5 kg meet the requirement. Therefore, it is only necessary to optimize the mobile platform parameters with geometry configurations that meet the requirement.

The minimal cable tension values and optimal mobile platform parameters for the corresponding geometry configuration obtained in the second phase are also displayed in Table 3. The optimal geometry configuration and mobile platform parameters are presented in Table 4 and illustrated in Figure 10b. The computation of the first phase took 4.5 h on a desktop computer with I7-4470-3.4Ghz, and the second phase was 40min on the same computer. Moreover, several other geometry configurations are provided in Table 2 and Table 3, and the corresponding performance indices are displayed. The no. 6 geometry configuration obtained after the first phase is also illustrated in Figure 10a as a comparison.

**TABLE 4. Optimal mobile platform parameters of no. 30 geometry configuration.**

| | Cable attachment positions | | | |
|---|---|---|---|---|
| | 5 | 6 | 7 | 8 |
| $W_p$(mm) | -62.5 | 62.5 | 62.5 | -62.5 |
| $D_p$(mm) | -77.5 | -77.5 | 77.5 | 77.5 |
| $H_p$(mm) | 192.5 | 192.5 | 192.5 | 192.5 |

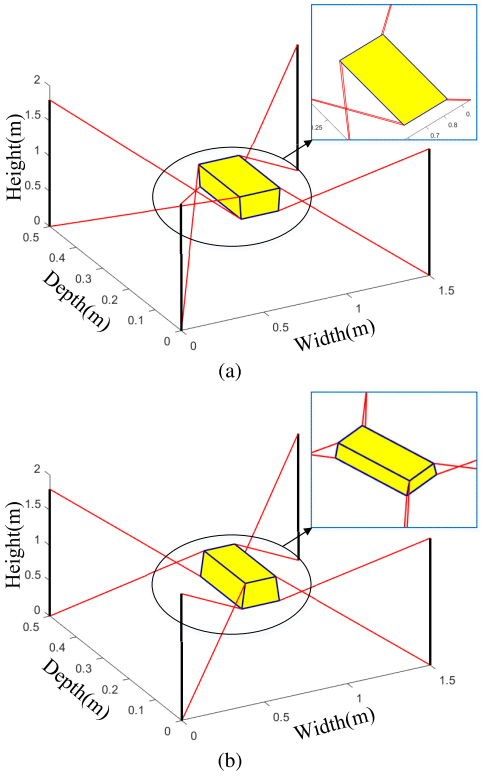


**FIGURE 10. Illustrations of geometry configurations: (a) no. 6 geometry configuration; (b) no. 30 geometry configuration.**

## VI. EXPERIMENTAL RESULTS

This section shows the simulation and static equilibrium experiment results for different geometry configurations and the mobile platform parameters.

### A. SIMULATION EXPERIMENT

A set of poses are selected to validate the maximal payload criterion and the minimal cable tension criterion of different geometry configurations for the 6-DOF RA-CDPR. The simulation test is carried out in the desired workspace and to analyze the distribution of the criterion at each pose. There are 10201 poses with uniform distribution in the desired workspace, and the criterion $m_{max}$ of each pose is calculated by Eq. (20). The distribution of the maximal payload ($m_{max}$) in the $X-Z$ plane of the two geometry configurations in the desired workspace are illustrated in Figure 11. The area surrounded by red lines represents 30kg $< m_{max}$, and the area surrounded by orange lines represents 3.5kg $< m_{max}$. The minimal cable tension criterion ($P_\tau$) and the desired workspace criterion ($P_w$) are shown in Figure 12.

From Figure 11a and Figure 11c, one can see that the $m_{max}$ of the No. 6 geometry configuration is obviously lower than that of the No. 30 geometry configuration in the central area, and the $m_{max}$ of the No. 30 geometry configuration is more than 62kg, while the $m_{max}$ of the No. 6 configuration is only about 45kg. In addition, the No. 30 configuration has a more uniform and symmetrical distribution of $m_{max}$ in the workspace. On the contrary, the No. 6 configuration has a partial mutation in different areas and its distribution in the workspace has no significant symmetry. The criterion $m_{max}$ of the No. 30 geometry configuration is poor close to the edge areas of the left and right sides of the desired workspace, and in some areas in the $m_{max} < 3.5$kg. Therefore, in these areas, the wrench-feasible condition cannot be satisfied. This point can also be supported by relevant conclusions from the Figure 12, in which one can find the desired workspace cannot be totally contained in the WFW of the No. 30 geometry configuration.

No.6-rnd denotes the minimal cable tension criterion ($P_\tau$) and the workspace criterion ($P_w$) of the No. 6 geometry configuration with randomly selected parameters of the mobile platform, as shown in Figure 12. Here, ''rnd'' refers to ''randomly selected parameters'' and the ''opt'' refers to ''optimal selected parameters''. These criteria can be calculated by solving Eq. (22) and Eq. (24). Moreover, No.6-opt describes the No. 6 geometry configuration with the optimal parameters of the mobile platform obtained from the second phase of the optimization process. Again, the meaning of No.30-rnd and No.30-opt can be explained similarly. It can be seen from Figure 12 that the minimal cable tension criterion of the No. 6 configuration and the No. 30 configuration with their optimized parameters are very close, but the workspace criterion of the No. 6 configuration is better than that of the No. 30 configuration. Meanwhile, the cable tension criterion ($P_\tau$) of the two configurations can be greatly improved by the optimization method.

### B. STATIC EQUILIBRIUM EXPERIMENT RESULTS

The proposed optimization method is validated on the RA-CDPR developed in our laboratory, as shown in Figure 13. The RA-CDPR consists of drive units, control cabinet, mobile platform, tension sensors and cables. The mobile platform of the RA-CDPR has 6-DOFs and can be moved by controlling the length and tension of cables in the workspace. A retractable fork is installed on the mobile platform, and the position of the retractable fork on the mobile platform can be adjusted arbitrarily. The drive units are modularized and can be arranged on the structure frame. Each drive unit comprises a servomotor, a planetary reducer and a winch unit. Moreover, several micro tension sensors are linked between the cables and the mobile platform to measure real cable tensions.

The base structure dimension of the RA-CDPR is 1800mm $\times$ 2000mm $\times$ 520mm ($W_s \times H_s \times D_s$). With the optimization method, the mobile platform parameters of No.30 configuration are optimized, and the optimal

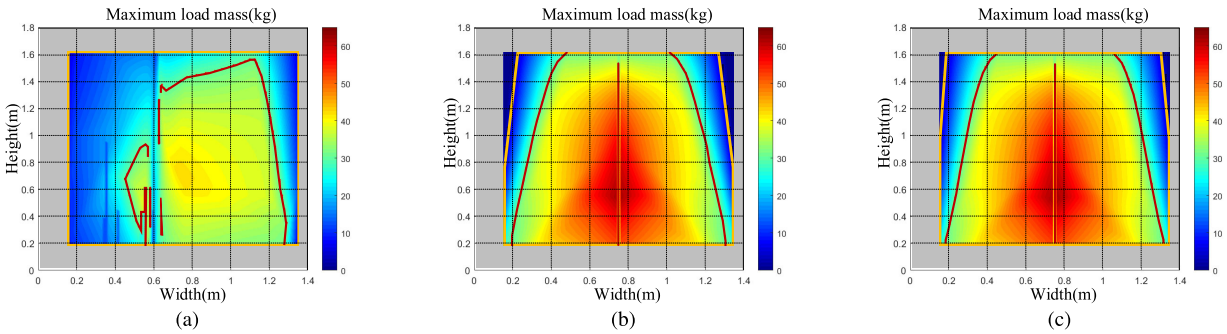


**FIGURE 11.** The distribution of the criterion $m_{max}$ on the $X-Z$ plane: (a) no. 6 geometry configuration; (b) no. 30 geometry configuration with optimal selected parameters which obtained from the first phase of the optimization algorithm; and (c) The No. 30 geometry configuration with optimization parameters which obtained from the second phase of the optimization algorithm.

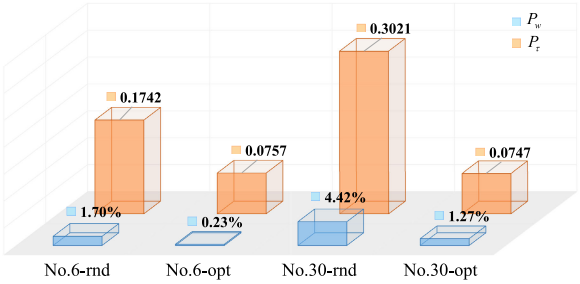


**FIGURE 12.** The minimal cable tension criterion and the desired workspace criterion in the simulation test.

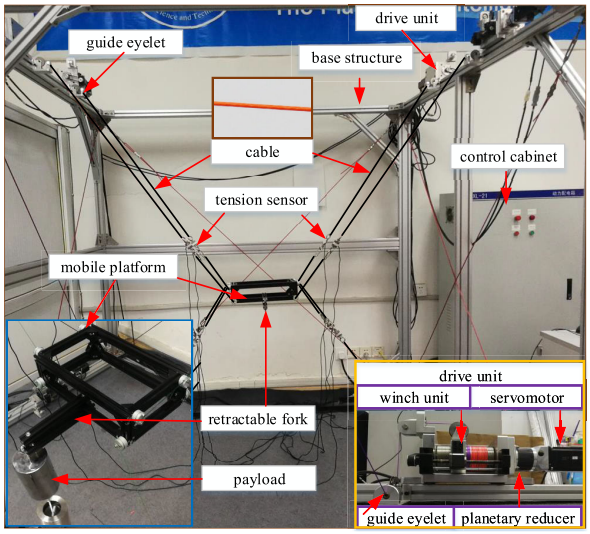


**FIGURE 13.** The RA-CDPR prototype.

parameters of $\{W_p, H_p\}$ are obtained as shown in Table 5. The geometric center of the base structure is used as the static equilibrium position to measure the cable tension under different payloads and geometry configurations, as shown in Figure 14. The distances between the mounting position of the payload on the retractable fork and the geometric center of the mobile platform are selected as $h = 0$mm, $h = 100$mm, $h = 200$mm. The mass of the mobile platform is 1.36kg, and the payload mass on the retractable fork are selected as 1kg, 2kg, 5kg, 7kg, 7.8kg, respectively. By the tension sensors,

**TABLE 5.** Optimization mobile platform parameters of the RA-CDPR prototype.

| | Cable attachment positions | | | |
|---|---|---|---|---|
| | 5 | 6 | 7 | 8 |
| $W_p$(mm) | -165 | 165 | 165 | -165 |
| $D_p$(mm) | -110 | -110 | 110 | 110 |
| $H_p$(mm) | 70 | 70 | 70 | 70 |

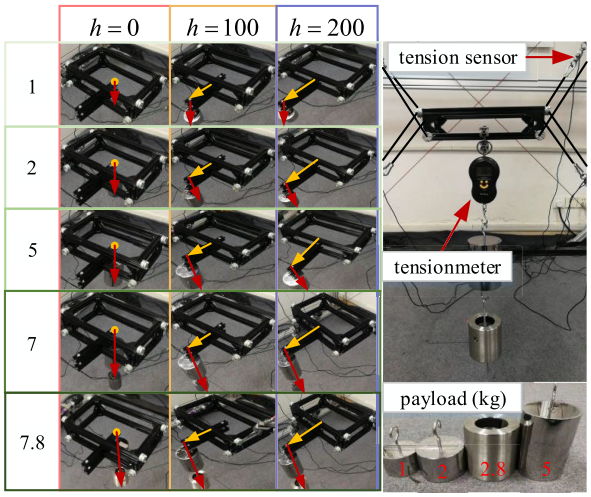


**FIGURE 14.** Static equilibrium test under different payloads and geometry configurations.

the cable tensions under different distances and payloads are obtained, as shown in Figure 15. After completing the static equilibrium test of the No. 30 configuration with the optimization parameters, the contrast geometry configuration is tested.

When the distance between the mounting position of the payload on the retractable fork and the geometric center of the mobile platform is $h = 0$mm, the CoG of the mobile platform and the payload coincides with the geometric center of the mobile platform, and the moment exerted by the payload on the mobile platform is very small. With the weight of the payload increases, the tensions on the suspended cables increase correspondingly. However, the cable tensions in the

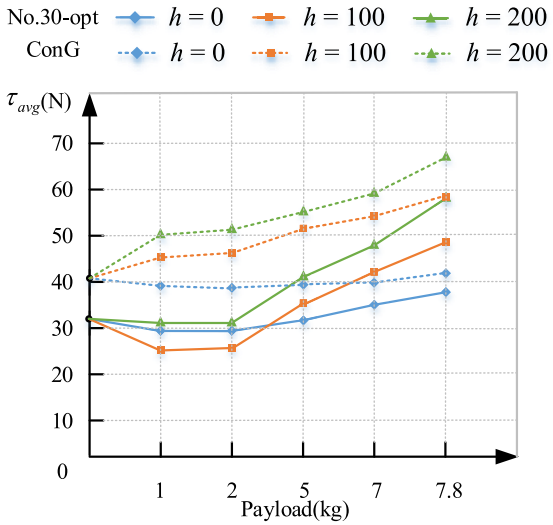


**FIGURE 15.** The average tension of cables under the No. 30 geometry configuration and the contrast geometry configuration. (No. 30-opt denotes the average tension of cables under the No. 30 geometry configuration; ConG denotes the average tension of cables under the contrast geometry configuration).

same direction as the gravity will decrease, resulting in a descent in the average tension of cables. When the weight of the payload is 0kg, the mobile platform is in the initial state, and the initial average tension of cables under the No. 30 configuration is less than that of the contrast geometry configuration. In general, the optimized geometry configuration and parameters have smaller average cable tension than the contrast geometry configuration, which is in line with the original intention of the design optimization.

## VII. CONCLUSION

This paper has presented a novel method for optimizing the geometry configurations and mobile platform parameters of RA-CDPRs in AWS. Based on the wrench-feasible condition, a new criterion defined as the maximal payload was introduced. Moreover, the other criterion, namely the minimal cable tension, was provided. The optimal geometry configuration and corresponding mobile platform parameters were obtained using the two-step optimization method. Furthermore, a simulation test was carried out. The simulation results demonstrated that the minimal cable tension of the no. 30 geometry configuration is very close to the optimal value. The no. 30 geometry configuration has the maximal payload index, and this index exhibits a more uniform and symmetric distribution in the workspace. In addition, static equilibrium tests were carried out on the No. 30 geometry configuration and the contrast geometry configuration. The average cable tension at different payload mass and center of gravity offset distance were measured. The test results show that the optimized geometry configuration can apply less cable tensions to balance the external forces and wrenches than the contrast geometry configuration. Thus, the optimization result offers the best overall performance and its geometry configuration is more suitable for RA-CDPRs in AWS. In future work, it is necessary to test the comprehensive performance of the RA-CDPR dynamically in the workspace.

## REFERENCES

[1] S. Seriani, M. Seriani, and P. Gallina, "Workspace optimization for a planar cable-suspended direct-driven robot," *Robot. Comput.-Integr. Manuf.*, vol. 34, pp. 1–7, Aug. 2015.
[2] H. Jamshidifar, A. Khajepour, B. Fidan, and M. Rushton, "Kinematically-constrained redundant cable-driven parallel robots: Modeling, redundancy analysis, and stiffness optimization," *IEEE/ASME Trans. Mechatronics*, vol. 22, no. 2, pp. 921–930, Apr. 2017.
[3] J. Lin, C. Y. Wu, and J. Chang, "Design and implementation of a multi-degrees-of-freedom cable-driven parallel robot with gripper," *Int. J. Adv. Robotic Syst.*, vol. 15, no. 5, Sep. 2018, Art. no. 172988141880384.
[4] S. Kawamura, W. Choe, S. Tanaka, and H. Kino, "Development of an ultra-high speed robot FALCON using parallel wire drive Systems.," *J. Robot. Soc. Jpn.*, vol. 15, no. 1, pp. 82–89, 1997.
[5] R. Yao, X. Tang, J. Wang, and P. Huang, "Dimensional optimization design of the four-cable-driven parallel manipulator in FAST," *IEEE/ASME Trans. Mechatronics*, vol. 15, no. 6, pp. 932–941, Dec. 2010.
[6] M. Gouttefarde, J.-F. Collard, N. Riehl, and C. Baradat, "Geometry selection of a redundantly actuated cable-suspended parallel robot," *IEEE Trans. Robot.*, vol. 31, no. 2, pp. 501–510, Apr. 2015.
[7] W. Wang, L. Yu, and J. Yang, "Linear parameter variant modeling and parameter identification of a cable-driven micromanipulator for surgical robot," *Proc. Inst. Mech. Eng. C, J. Mech. Eng. Sci.*, vol. 233, no. 5, pp. 1828–1840, Mar. 2019.
[8] B. Zi, B. Wang, and D. Wang, "Design and analysis of a novel cable-actuated palletizing robot," *Int. J. Adv. Robotic Syst.*, vol. 14, no. 6, Nov. 2017, Art. no. 172988141774108.
[9] W. Zhang, W. Shang, B. Zhang, F. Zhang, and S. Cong, "Stiffness-based trajectory planning of a 6-DOF cable-driven parallel manipulator," *Proc. Inst. Mech. Eng. C, J. Mech. Eng. Sci.*, vol. 231, no. 21, pp. 3999–4011, 2017.
[10] M. Hassan and A. Khajepour, "Analysis of a large-workspace cable-actuated manipulator for warehousing applications," in *Proc. Int. Design Eng. Tech. Conf., Comput. Inf. Eng. Conf. (ASME)*. San Diego, CA, USA: American Society of Mechanical Engineers, Aug. 2009, pp. 45–53.
[11] M. Ramadan, B. Salah, and B. Noche, "Innovative estimating travel time model for dual-command cycle time of Stewart-Gough platform in automated storage/retrieval systems," in *Proc. Int. Design Eng. Tech. Conf. Comput. Inf. Eng. Conf. (ASME)*. Chicago, IL, USA: American Society of Mechanical Engineers, Aug. 2012, pp. 737–743.
[12] T. Bruckmann, C. Sturm, L. Fehlberg, and C. Reichert, "An energy-efficient wire-based storage and retrieval system," in *Proc. IEEE/ASME Int. Conf. Adv. Intell. Mechatronics (AIM)*. Wollongong, NSW, Australia: IEEE, Aug. 2013, pp. 631–636.
[13] T. Bruckmann, C. Reichert, and H. Ji, "Energy consumption reduction of a cable-driven storage and retrieval system," in *Advances in Robot Kinematics*. Cham, Switzerland: Springer, Jun. 2018, pp. 383–391.
[14] W. Wang, X. Tang, and Z. Shao, "Study on energy consumption and cable force optimization of cable-driven parallel mechanism in automated storage/retrieval system," in *Proc. 2nd Int. Conf. Soft Comput. Mach. Intell. (ISCMI)*. Hongkong, China: IEEE, Nov. 2015, pp. 144–150.
[15] H. Jamshidifar, B. Fidan, G. Gungor, and A. Khajepour, "Adaptive vibration control of a flexible cable driven parallel robot," *IFAC-PapersOnLine*, vol. 48, no. 3, pp. 1302–1307, 2015.
[16] H. Jamshidifar, S. Khosravani, B. Fidan, and A. Khajepour, "Vibration decoupled modeling and robust control of redundant cable-driven parallel robots," *IEEE/ASME Trans. Mechatronics*, vol. 23, no. 2, pp. 690–701, Apr. 2018.
[17] M. Rushton, H. Jamshidifar, and A. Khajepour, "Multiaxis reaction system (MARS) for vibration control of planar cable-driven parallel robots," *IEEE Trans. Robot.*, vol. 35, no. 4, pp. 1039–1046, Aug. 2019.
[18] M. Hassan and A. Khajepour, "Optimization of actuator forces in cable-based parallel manipulators using convex analysis," *IEEE Trans. Robot.*, vol. 24, no. 3, pp. 736–740, Jun. 2008.
[19] Y. Mao and S. K. Agrawal, "Design of a cable-driven arm exoskeleton (CAREX) for neural rehabilitation," *IEEE Trans. Robot.*, vol. 28, no. 4, pp. 922–931, Aug. 2012.
[20] J. T. Bryson, X. Jin, and S. K. Agrawal, "Optimal design of cable-driven manipulators using particle swarm optimization," *J. Mech. Robot.*, vol. 8, no. 4, Aug. 2016, Art. no. 041003.

[21] B. Zhang, W.-W. Shang, S. Cong, and Y. Liu, "Size optimization of the moving platform for cable-driven parallel manipulators based on stiffness characteristics," *Proc. Inst. Mech. Eng. C, J. Mech. Eng. Sci.*, vol. 232, no. 11, pp. 2057–2066, Jun. 2018.
[22] S. Abdolshah, D. Zanotto, G. Rosati, and S. K. Agrawal, "Optimizing stiffness and dexterity of planar adaptive cable-driven parallel robots," *J. Mech. Robot.*, vol. 9, no. 3, Jun. 2017, Art. no. 031004.
[23] R. Williams, II, B. Snyder, J. S. Albus, and R. V. Bostelman, "Seven-DOF cable-suspended robot with independent metrology," in *Proc. Int. Design Eng. Tech. Conf. Comput. Inf. Eng. Conf. (ASME)*. Salt Lake City, UT, USA: American Society of Mechanical Engineers, Sep. 2004, pp. 317–325.
[24] P. Gallina and G. Rosati, "Manipulability of a planar wire driven haptic device," *Mechanism Mach. Theory*, vol. 37, no. 2, pp. 215–228, Feb. 2002.
[25] C. Ferraresi, M. Paoloni, S. Pastorelli, and F. Pescarmona, "A new 6-DOF parallel robotic structure actuated by wires: The WiRo-6.3," *J. Robotic Syst.*, vol. 21, no. 11, pp. 581–595, Nov. 2004.
[26] J. Pusey, A. Fattah, S. Agrawal, and E. Messina, "Design and workspace analysis of a 6–6 cable-suspended parallel robot," *Mechanism Mach. Theory*, vol. 39, no. 7, pp. 761–778, 2004.
[27] S. Tadokoro, Y. Murao, M. Hiller, R. Murata, H. Kohkawa, and T. Matsushima, "A motion base with 6-DOF by parallel cable drive architecture," *IEEE/ASME Trans. Mechatronics*, vol. 7, no. 2, pp. 115–123, Jun. 2002.
[28] F. Hao and J.-P. Merlet, "Multi-criteria optimal design of parallel manipulators based on interval analysis," *Mechanism Mach. Theory*, vol. 40, no. 2, pp. 157–171, Feb. 2005.
[29] Y. Lou, Y. Zhang, R. Huang, X. Chen, and Z. Li, "Optimization algorithms for kinematically optimal design of parallel manipulators," *IEEE Trans. Autom. Sci. Eng.*, vol. 11, no. 2, pp. 574–584, Apr. 2014.
[30] R. Baños, C. Gil, B. Paechter, and J. Ortega, "A hybrid meta-heuristic for multi-objective optimization: MOSATS," *J. Math. Model. Algorithms*, vol. 6, no. 2, pp. 213–230, May 2007.
[31] J. Branke, J. Branke, K. Deb, K. Miettinen, and R. Slowinski, *Multiobjective Optimization: Interactive and Evolutionary Approaches*, vol. 5252. Springer, 2008.
[32] C. Gil, A. Márquez, R. Baños, M. G. Montoya, and J. Gómez, "A hybrid method for solving multi-objective global optimization problems," *J. Global Optim.*, vol. 38, no. 2, pp. 265–281, May 2007.
[33] N. V. Thoai, "Criteria and dimension reduction of linear multiple criteria optimization problems," *J. Global Optim.*, vol. 52, no. 3, pp. 499–508, Mar. 2012.
[34] A. Pott, T. Bruckmann, and L. Mikelsons, "Closed-form force distribution for parallel wire robots," in *Computational Kinematics*. Berlin, Germany: Springer, 2009, pp. 25–34.
[35] J. Currie, N. Sahinidis, J. Pinto, and D. I. Wilson, "OPTI: Lowering the barrier between open source optimizers and the industrial MATLAB user," in *Foundations of Computer-Aided Process Operations*, N. Sahinidis and J. Pinto, Eds. Savannah, GA, USA, Jan. 2012, pp. 8–11.
[36] S. Bouchard, C. Gosselin, and B. Moore, "On the ability of a cable-driven robot to generate a prescribed set of wrenches," *J. Mech. Robot.*, vol. 2, no. 1, pp. 47–58, 2010.
[37] D. Nguyen and M. Gouttefarde, "On the improvement of cable collision detection algorithms," in *Cable-Driven Parallel Robots*, vol. 32. Berlin, Germany: Springer, 2015, pp. 29–40.
[38] F. Glover, "Future paths for integer programming and links to artificial intelligence," *Comput. Oper. Res.*, vol. 13, no. 5, pp. 533–549, Jan. 1986.
[39] J. C. Weis, B. Ernst, and K.-H. Wehking, "Use of high strength fibre ropes in multi-rope kinematic robot systems," in *Cable-Driven Parallel Robots*. Berlin, Germany: Springer, 2013, pp. 185–199.

**FEI ZHANG** received the B.E. degree from the Department of Mechanical Engineering, Anhui University of Science and Technology, in 2012. He is currently pursuing the Ph.D. degree with the University of Science and Technology of China. His research interests include parameter calibration and the optimal design of robots.

**WEIWEI SHANG** (Senior Member, IEEE) received the Ph.D. degree in control science and engineering from the University of Science and Technology of China, in 2008. He is currently an Associate Professor with the Department of Automation, University of Science and Technology of China. His current research interests include parallel robots, cable-driven robots, humanoid robots, and robotic learning control.

**BIN ZHANG** received the B.E. degree in automation from the University of Science and Technology of China, in 2013, where he is currently pursuing the Ph.D. degree. His research interests include the optimal design and dynamic control of parallel robots.

**SHUANG CONG** received the B.S. degree in automatic control from the Beijing University of Aeronautics and Astronautics, in 1982, and the Ph.D. degree in system engineering from the University of Rome "La Sapienza", Rome, Italy, in 1995. She is currently a Professor with the Department of Automation, University of Science and Technology of China. Her research interests include advanced control, fuzzy logic control, neural networks, and quantum system control.